



1 **Determination of the atmospheric lifetime and global**
2 **warming potential of sulphur hexafluoride using a three-**
3 **dimensional model**

4 Tamás Kovács¹, Wuhu Feng^{1,2}, Anna Totterdill¹, John M.C. Plane¹, Sandip Dhomse²,
5 Juan Carlos Gómez-Martín¹, Gabriele P. Stiller³, Florian J. Haenel³, Christopher Smith⁴,
6 Piers M. Forster², Rolando R. García⁵, Daniel R. Marsh⁵ and Martyn P. Chipperfield^{2*}

7 ¹School of Chemistry, University of Leeds, Leeds LS2 9JT, UK.

8 ²NCAS, School of Earth and Environment, University of Leeds, Leeds LS2 9JT, UK.

9 ³Karlsruhe Institute of Technology, IMK-ASF, PO BOX 3640, 76021 Karlsruhe, Germany.

10 ⁴Energy Research Institute, School of Chemical and Process Engineering, University of Leeds,
11 Leeds LS2 9JT, UK.

12 ⁵National Center for Atmospheric Research (NCAR), Boulder, Colorado, USA.

13 *Correspondence to: Martyn Chipperfield (M.Chipperfield@leeds.ac.uk)

14 **Abstract.** We have used the Whole Atmosphere Community Climate Model (WACCM), with
15 an updated treatment of loss processes, to determine the atmospheric lifetime of SF₆. The model
16 includes the following SF₆ removal processes: photolysis, electron attachment and reaction
17 with mesospheric metal atoms. The Sodankylä Ion Chemistry (SIC) model is incorporated into
18 the standard version of WACCM to produce a new version with a detailed *D* region ion
19 chemistry with cluster ions and negative ions. This is used to determine a latitude- and altitude-
20 dependent scaling factor for the electron density in the standard WACCM in order to carry out
21 multi-year SF₆ simulations. The model gives a mean SF₆ lifetime over a 11-year solar cycle (τ)
22 of 1278 years (with a range from 1120 to 1475 years), which is much shorter than the currently
23 widely used value of 3200 years, due to the larger contribution (97.4%) of the modelled
24 electron density to the total atmospheric loss. The loss of SF₆ by reaction with mesospheric
25 metal atoms (Na and K) is far too slow to affect the lifetime. We investigate how this shorter
26 atmospheric lifetime impacts the use of SF₆ to derive stratospheric age-of-air. The age-of-air
27 derived from this shorter lifetime SF₆ tracer is longer by 9% in polar latitudes at 20 km
28 compared to a passive SF₆ tracer. We also present laboratory measurements of the infrared
29 spectrum of SF₆ and find good agreement with previous studies. We calculate the resulting
30 radiative forcings and efficiencies to be, on average, very similar to those reported previously.
31 Our values for the 20, 100 and 500-year global warming potentials are 18,000, 23,800 and
32 31,300, respectively.



33 **1 Introduction**

34 Sulphur hexafluoride (SF₆) is an anthropogenic greenhouse gas which is mainly used as an
35 electrical insulator, with other applications as a quasi-inert gas. Although its main sources are
36 in the Northern Hemisphere, its atmospheric abundance is increasing globally in response to
37 these emissions and its long atmospheric lifetime. SF₆ is characterised by large absorption
38 cross-sections for terrestrial infrared radiation such that the presently increasing SF₆ abundance
39 will contribute a positive radiative forcing over many centuries. The important known removal
40 sources are electron attachment and photolysis. Recently, we have also measured bimolecular
41 rate constants for the reaction of SF₆ with mesospheric metals (Totterdill *et al.*, 2015).

42 Harnisch and Eisenhauer (1998) reported that SF₆ is naturally present in fluorites, and out-
43 gassing from these materials leads to a natural background atmospheric abundance of 0.01
44 pptv. However, at present the anthropogenic emissions of SF₆ exceed the natural ones by a
45 factor of 1000 or more and are responsible for the rapid increase in its atmospheric abundance.
46 Surface measurements show that SF₆ increased by about 7%/year during the 1980s and 1990s
47 (Geller *et al.*, 1997; Maiss and Brenninkmeijer, 1998).

48 SF₆ provides a useful tracer of atmospheric transport in both the troposphere and stratosphere.
49 Rates for transport of pollutants into, within, and out of the stratosphere are important
50 parameters that regulate stratospheric composition. The basic characteristics of the
51 stratospheric Brewer-Dobson (B-D) circulation are known from observations of trace gases
52 such as SF₆: air enters the stratosphere at the tropical tropopause, rises at tropical latitudes, and
53 descends at middle and high latitudes to return to the troposphere. Understanding the rate of
54 this transport on a global scale is crucial in order to predict the response of stratospheric ozone
55 to climatic or chemical change. SF₆ is essentially inert in the troposphere to middle stratosphere
56 and is removed by electron attachment and photolysis in the upper stratosphere and mesosphere
57 (Ravishankara *et al.*, 1993). This tracer therefore provides an ideal probe of transport on
58 timescales of importance in the stratospheric circulation and quantitative information on mean
59 air mass age for the lower and middle stratosphere.

60 The mean age-of-air (AoA) is the interval between the time when the volume mixing ratio of
61 a linearly increasing atmospheric tracer reaches a certain value at a given location in the
62 stratosphere and an earlier time when this mixing ratio was reached at a reference location.
63 Mean AoA is expressed as (Hall and Plumb, 1994; Waugh and Hall, 2002)



$$64 \quad \text{AoA} = t(\chi, l, z) - t(\chi, l_0, z_0) \quad (E1)$$

65 where t is time, χ is the volume mixing ratio, l and z are latitude and altitude, and the 0 subscripts
66 denote the reference latitude and altitude which are chosen to be the upper tropical troposphere
67 (latitude = 1°N, altitude = 13.9 km). In principle the trend of AoA can be used to diagnose
68 changes in the strength of Brewer-Dobson circulation (BDC); in practice, however, it is very
69 difficult to obtain unambiguous results on trends from this or any other trace gas (Garcia *et al.*,
70 2011). Ideally, AoA should be determined experimentally using a tracer with very small (or
71 zero) chemical sink in the stratosphere or mesosphere. Otherwise, a correction must be applied
72 to account for this loss. A correction would also be necessary for any non-linear tropospheric
73 growth. However, for the period considered for diagnosing age-of-air in this paper (2002-2007)
74 the growth of SF₆ is approximately linear, so we can reasonably neglect such a correction for
75 SF₆-derived AoA (Hall and Plumb, 1994).

76 Ravishankara *et al.* (1993) reported the atmospheric lifetime of SF₆ to be 3200 years by
77 considering electron attachment and vacuum ultraviolet (VUV) photolysis. They also studied
78 the loss of SF₆ by reaction with O(¹D) but found the rate too slow to be important. They
79 deduced that electron attachment was the dominant loss process and quantified this process
80 using a 2-D model, wherein they assumed that all SF₆ molecules are destroyed after attachment
81 of an electron (with a rate constant of 10⁻⁹ cm³ molecule⁻¹ s⁻¹). They therefore argued that their
82 lifetime of 3200 years could be a lower limit, but clearly this result depends on the accuracy of
83 the 2-D electron density, which was calculated using only photochemistry. Morris *et al.* (1995)
84 subsequently extended the work of Ravishankara *et al.* (1993) by including an ion chemistry
85 module in the same 2-D model. They also made other assumptions to maximise the impact of
86 electron attachment on SF₆ loss and derived a lifetime as low as 800 years (which could be
87 further sporadically decreased by large solar proton events). Using a 3-D middle atmosphere
88 model, Reddman *et al.* (2001) estimated the lifetime to be 472 years when SF₆ is irreversibly
89 destroyed purely by direct electron attachment and to be 9379 years when SF₆ loss is assumed
90 to occur only via indirect loss (via the formation of SF₆⁻) and ionization via the reactions with
91 O₂⁺ and N₂⁺. They concluded that the estimated lifetime depends strongly on the electron
92 attachment mechanism, because the efficiency of this process as a permanent removal process
93 of SF₆ depends on the competition between reaction of SF₆⁻ with H and HCl, and
94 photodetachment and reaction with O and O₃. Here we extend on the above studies and
95 investigate the SF₆ lifetime using a state-of-the-art 3-D chemistry climate model with a domain



96 from the surface to 140 km. Our modelled electron density is based on results of a detailed ion
97 chemistry model and we use a detailed methodology for treating the atmospheric background
98 electrons, which is based on Troe's formalism (Troe *et al.*, 2007a,b; Viggiano *et al.*, 2007).

99 In addition to determining the SF₆ lifetime, in this study we report new measurements of the
100 infrared absorption cross-sections for SF₆ and input these into a line-by-line radiative transfer
101 model in order to obtain radiative forcings and efficiencies. These values are then used to
102 determine more accurate values of global warming potentials (GWPs) based on their cloudy
103 sky adjusted radiative efficiencies. GWP is the metric used by the World Meteorological
104 Organisation (WMO) and Intergovernmental Panel on Climate Change (IPCC) to compare the
105 potency of a greenhouse gas relative to an equivalent emission of CO₂ over a set time period.
106 The definitions of these radiative terms are discussed in detail in our recent publication
107 Totterdill *et al.* (2016).

108 **2 Methodology**

109 **2.1 WACCM 3D model**

110 To simulate atmospheric SF₆ we have used the Whole Atmosphere Community Climate Model
111 (WACCM). Here we use WACCM 4 (Marsh *et al.*, 2013), which is part of the NCAR
112 Community Earth System Model (CESM; Lamarque *et al.*, 2012), configured to have 88
113 pressure levels from the surface to the lower thermosphere (5.96×10^{-6} Pa, 140 km) and a
114 horizontal resolution of $1.9^\circ \times 2.5^\circ$ (latitude \times longitude). The model contains a detailed
115 treatment of middle atmosphere chemistry including interactive treatments of Na and K (Plane
116 *et al.*, 2015). We use the specified dynamics (SD) version of the model to allow comparison
117 with observations (see Garcia *et al.*, (2014) for details). The SF₆ surface emission flux and
118 initial global vertical profiles were taken from a CCMI (Chemistry Climate Model Initiative)
119 simulation using the same version of SD-WACCM with the same nudging analyses (D.
120 Kinnison, personal communication, 2013).

121 Lyman- α photolysis is the only SF₆ loss reaction in the standard version of WACCM and in
122 this work we have added the additional processes given in **Table 1**. The rate constants for the
123 SF₆ + metal reactions have been measured in our laboratory for mesospheric conditions
124 (Totterdill *et al.*, 2015); here we use the experimental values for the reactions with Na and K.
125 For the photolysis of SF₆ we used the standard WACCM methodology but with the updated
126 Lyman- α cross section from our laboratory of 1.37×10^{-18} cm² molecule⁻¹ (Totterdill *et al.*,
127 2015). The WACCM Lyman- α flux is taken from Chabrilat and Kockarts (1997).



128 Electron attachment to SF₆ plays a major role in its atmospheric removal and so both
 129 dissociative and non-dissociative attachment are considered in this study. The detailed method
 130 is described in a recent paper (Totterdill *et al.*, 2015) and here only a brief summary is given.
 131 The removal process by the attachment of low energy electrons to SF₆ can be described using
 132 Troe's theory (Troe *et al.*, 2007a,b; Viggiano *et al.*, 2007). In the middle and lower mesosphere,
 133 electrons are mostly attached to neutral species in the form of anions. However, above 80 km
 134 the concentration of free electrons increases and the direct electron attachment to SF₆ becomes
 135 more likely. This can happen either by associative attachment forming the SF₆⁻ anion which
 136 can then undergo chemical reactions with H, O, O₃ and HCl, or by dissociative attachment
 137 forming the SF₅⁻ anion fragment. The probability β of dissociative attachment when an electron
 138 is captured by SF₆ is given by

$$139 \quad \beta(p, T) = \frac{k_{dis}}{k_{at} + k_{dis}} \quad (E2)$$

140 where k_{dis} is the rate constant for dissociative attachment and k_{at} is the rate constant for
 141 associative attachment. β can be expressed as

$$142 \quad \beta(p, T) = \exp(-4587T + 7.74) \times 10^{\left[4.362 - 0.582 \log_{10}(p/Torr) - 0.0203 \left(\log_{10}\left(\frac{p}{Torr}\right)\right)^2\right] / 5.26 \times 10^{-4}} \quad (E3)$$

144 where T is the temperature in K and p is the pressure in Torr (Totterdill *et al.*, 2015).

145 We include both associative and dissociative electron attachment using WACCM-predicted
 146 electron concentrations (see **Table 1**). Note that the SF₆⁻ anion is not modelled directly. Instead
 147 the SF₆ attachment loss rate is calculated by multiplying k_{at} by the probability of permanent
 148 destruction of the resulting SF₆⁻ (reactions of SF₆⁻ with H and HCl) to the sum of these reactions
 149 and processes which recycle SF₆⁻ to SF₆ (reactions with O and O₃, and photodetachment)
 150 (Morris *et al.*, 1995).

151 In order to use a realistic electron concentration, the role of negative ions in the D region must
 152 be considered. Therefore, a scaling factor was introduced that converts the standard WACCM
 153 electron concentrations, which are calculated from charge balance with the five major positive
 154 E region ions (N⁺, N₂⁺, O⁺, O₂⁺ and NO⁺), to more realistic electron concentrations. We have
 155 recently incorporated the Sodankylä Ion Chemistry (SIC) model into the standard version of
 156 WACCM to produce a new version (WACCM-SIC) containing a detailed D region ion



157 chemistry with cluster ions and negative ions (Kovács *et al.*, 2016). The mesospheric positive
158 and negative ions in WACCM-SIC are listed in **Table 2**. The electron scaling factor in each
159 grid box of WACCM was then defined as the annually averaged ratio of $[e]_{\text{WACCM-SIC}}/[e]_{\text{WACCM}}$
160 for the year 2013, where $[e]_{\text{WACCM-SIC}}$ is the electron density calculated from WACCM-SIC
161 and $[e]_{\text{WACCM}}$ from the standard WACCM.

162 The scaling factor, which varies with altitude and latitude, is shown in **Figure 1** (bottom panel)
163 together with the electron densities from the standard WACCM (top panel) and WACCM-SIC
164 (middle panel) models. The annually averaged electron concentration in the WACCM-SIC
165 model is significantly smaller in the lower and middle mesosphere than in the standard
166 WACCM, which is expected because of negative ion formation. Note that in the upper
167 mesosphere (70 - 80 km) the electron density in WACCM-SIC is larger than WACCM. This
168 results from the inclusion of medium energy electrons (MEE) (electrons with energy between
169 30 keV and 2MeV) in WACCM-SIC. **Figure 2** shows the effect of MEE by comparing
170 WACCM-SIC runs with and without this source of ionization in the upper mesosphere
171 included. To describe the effect of ionization, WACCM-SIC uses ionization rates (I) as a
172 function of time and pressure which were calculated from the spectra based on the proton
173 energy-range measurements in standard air as described by Verronen *et al.* (2005). According
174 to Figure 3 of Meredith *et al.* (2015), the annually averaged medium energy electron flux for
175 2013 approximately corresponds to the long-term, 20-year average. This allows us to assume
176 that the annually averaged electron density of 2013 from WACCM-SIC can be used to scale
177 the long-term simulations using the standard WACCM aimed at determining the atmospheric
178 lifetime of SF₆.

179 The WACCM simulation included five different SF₆ tracers in order to quantify the importance
180 of different loss processes. All of these tracers used the same emissions but differed in their
181 treatment of SF₆ loss reactions. One SF₆ tracer included no atmospheric loss (i.e. a passive
182 tracer). Three tracers included one of the following loss processes for SF₆: (i) reaction with
183 mesospheric metals (Na, K), (ii) electron attachment, and (iii) UV photolysis. Finally, one ‘total
184 reactive’ SF₆ tracer included all three loss processes. This total reactive tracer should be the
185 most realistic and was used in the radiative forcing calculations. WACCM was run for the
186 period 1990-2007, and the first five years were treated as spin-up. For the analysis the monthly
187 mean model outputs were saved and later globally averaged for the lifetime calculations.

188



189 2.2 Infrared absorption spectrum and radiative forcing

190 Previous quantitative infrared absorption spectra of SF₆ have been compared in Hodnebrog *et*
191 *al.* (2013) (their Table 12). There are differences of ~10% between existing integrated cross-
192 section estimates, and the measurements cover different spectral ranges. We therefore
193 performed a more complete set of measurements over a wider spectral range, in order to reduce
194 uncertainty in the absorption spectrum and hence the radiative efficiency of SF₆. Measurements
195 were taken using an experimental configuration consisting of a Bruker Fourier transform
196 spectrometer (Model IFS/ 66), which was fitted with a mid-infrared (MIR) source used to
197 generate radiation which passed through an evacuable gas cell with optical path length 15.9
198 cm. The cell was fitted with KBr windows, which allow excellent transmission between 400
199 and 40,000 cm⁻¹. The choice of source and window were selected so as to admit radiation across
200 the mid IR range where bands of interest are known to occur. Room temperature (296 ± 2 K)
201 measurements were carried out between 400 and 2000 cm⁻¹ at a spectral resolution of 0.1 cm⁻¹
202 and compiled from the averaged total of 128 scans to 32 background scans at a scanner velocity
203 of 1.6 kHz. Gas mixtures were made using between 8 and 675 Torr of SF₆ diluted up to an
204 atmosphere using N₂, according to the method described in Totterdill *et al.* (2016).

205 Radiative forcing calculations were made using the Reference Forward Model (RFM) (Dudhia,
206 2013) which is a line-by-line radiative transfer model based on the previous GENLN2 model
207 (Edwards, 1987). Results obtained from this model were validated against the DISORT
208 radiative transfer solver (Stamnes *et al.*, 2000) included within the libRadtran (Library for
209 Radiative Transfer) package (Mayer and Kylling, 2005). A full description of these models and
210 parameters used alongside discussion of treatment of clouds and model comparison is also
211 given in Totterdill *et al.* (2016).

212 3 Results

213 3.1 Global distributions of SF₆ from WACCM simulations

214 **Figure 3** shows typical zonal mean profiles of the WACCM SF₆ tracers in the north and south
215 polar regions for different seasons, compared to MIPAS observations for the year 2007 (Haenel
216 *et al.*, 2015). Although the MIPAS SF₆ data provides much more coverage horizontally and
217 vertically compared to in situ aircraft and balloon data, it has only been validated up to 35 km
218 (Stiller *et al.*, 2008). At higher altitudes validation is not possible due to the lack of suitable
219 reference data. Details of the validation of the MIPAS data version used here (V5h_SF6_20
220 for the full resolution product from 2004 and earlier; V5r_SF6_222 and V5r_SF6_223 for the



221 reduced resolution period of 2005 and later) can be found in Haenel *et al.* (2015), including
222 Figure S-2 of their supplementary material. The WACCM passive SF₆ tracer has a mixing ratio
223 profile that is fairly constant with altitude until around 70 km, after which it decreases.
224 Comparison of the tracers that include loss processes show that removal of SF₆ is dominated
225 by electron attachment, with a small contribution direct from photolysis. The mesospheric
226 metals make a negligible contribution because the Na and K layers occur in the upper
227 mesosphere above 80 km (with peaks around 90 km), and the concentrations of these metal
228 atoms are too low. As is clear from **Figure 3**, the model simulation and satellite observations
229 agree within the atmospheric variability, which becomes relatively large above 30 km
230 especially at high latitudes, although the model is systematically larger than the observations
231 above 20 km. The time variation of modelled SF₆ shown in **Figure 4** corresponds to an
232 emission rate (slope) of 6.5×10^{-3} Tg/year, i.e. a 0.29 pptv/year increase in global mean volume
233 mixing ratio, and a volume mixing ratio of 6.4 pptv by the end of 2007.

234 **Figure 5** shows the zonal mean annual mean SF₆ distribution from the five WACCM tracers
235 and MIPAS observations for 2007. **Figure 5a** (and **Figure 3**) shows that there is a rapid
236 decrease in SF₆ above 75 km even for the inert tracer. This can be explained by diffusive
237 separation, which becomes pronounced in the upper mesosphere because SF₆ is a relatively
238 heavy molecule compared to the mean molecular mass of air molecules (cf. Garcia *et al.* (2014),
239 where similar behaviour is seen for CO₂, another relatively heavy molecule). Panels (a)-(c) of
240 the figure all show SF₆ decreasing above ~80 km, and panels (a) and (c) are almost identical,
241 while in panel (b) the decrease begins a little lower. This is all consistent with the notion that
242 metals do not affect SF₆ and photolysis contributes only slightly. The fact that diffusive
243 separation prevents SF₆ from reaching altitudes where photolysis is faster must be contributing
244 to the very long lifetime found when photolysis is the only loss considered. By contrast, in
245 **Figure 5d** SF₆ decreases rapidly above 70 km, which is related to the fact that loss via electron
246 attachment is important at these lower altitudes. Thus, in this case, SF₆ loss occurs below the
247 altitudes where diffusive separation is important (and where air density is higher), which makes
248 it a much more effective loss mechanism. The WACCM SF₆ tracer that includes all loss
249 processes (**Figure 5e**) has a very similar distribution to that which only treats loss due to
250 electron attachment (**Figure 5d**), which emphasises how this process dominates SF₆ loss in the
251 model. This model tracer can be compared to the MIPAS observations in **Figure 5f**, which
252 shows that WACCM agrees reasonably well with the measurements in the lower stratosphere
253 (note the smaller altitude range in panels (e) and (f) of **Figure 5**). Finally, it is also clear that



254 WACCM SF₆, even with all losses considered, decreases with altitude much more slowly at all
255 latitudes than MIPAS SF₆. This could indicate a problem with the model's meridional transport.
256 However, a too-fast BDC would tend to produce low levels of SF₆ at middle and high latitudes
257 in the descending branch, which does not seem to be the case. Therefore, at least two other
258 possible scenarios could be responsible for the discrepancy: SF₆ loss in WACCM is still
259 somewhat underestimated despite the inclusion of the electron attachment, or MIPAS SF₆ is
260 biased low above ~20 km.

261 3.2 Atmospheric lifetime

262 The atmospheric lifetime is defined as the ratio of the atmospheric burden to the atmospheric
263 loss rate. This definition was used to calculate annual mean lifetime values from the WACCM
264 output containing the individual rates for the different loss processes. During the simulation
265 the total atmospheric burden of SF₆ increased linearly as expected (see **Figure 4**) from 3.4×10^{32}
266 molecules with an annual increment of 2.3×10^{31} molecules/year. **Figure 6** shows the variation
267 in SF₆ lifetime from 1995 to 2007, corresponding to a full solar cycle (the solar minima
268 occurred in May 1996 and January 2008). The figure demonstrates that the lifetime has a strong
269 dependence on solar activity, being anti-correlated with the solar radio flux at 10.7 cm (2800
270 MHz) (Tapping, 2013) which ranges over $(72 - 183) \times 10^{-22} \text{ W m}^{-2} \text{ Hz}^{-1}$, with an average value
271 of $90.3 \times 10^{-22} \text{ W m}^{-2} \text{ Hz}^{-1}$. The mean SF₆ lifetime and range over the same solar cycle period τ
272 = 1278 years, with a range from 1120 to 1475 years. The annual averaged electron number
273 density in the polar regions is also plotted in **Figure 6**; as expected, it is correlated with the
274 10.7 cm radio emission (Tapping, 2013).

275 As noted in the Introduction, the SF₆ lifetime has been reported to be 3200 years by
276 Ravishankara *et al.*, (1993). For this they used a total electron attachment rate constant of k_{EA}
277 = $10^{-9} \text{ cm}^3 \text{ s}^{-1}$. In Morris *et al.* (1995) the calculated lifetime decreased to 800 years by
278 considering ion chemistry and assuming that the associative attachment forming SF₆⁻ does not
279 regenerate the parent molecule, thereby obtaining a lower limit for the lifetime. Reddmann *et*
280 *al.* (2001) estimated the lifetime to be 472 yr when SF₆ is irreversibly destroyed purely by
281 direct electron attachment and to be 9379 yr when SF₆ loss is assumed to occur only via indirect
282 loss (via the formation of SF₆⁻) and ionization via the reactions with O₂⁺ and N₂⁺. In the present
283 study we have directly applied Troe's theory (Troe *et al.*, 2007a,b; Viggiano *et al.*, 2007) to
284 determine the efficiency of electron attachment as a function of temperature and pressure, and



285 the branching ratio for dissociative attachment (equation E2), which we extrapolated to
286 mesospheric conditions (Totterdill *et al.*, 2015).

287 Our estimated *partial* lifetime of SF₆ due to photolysis for the SF₆ tracer which includes all
288 loss processes is 48,000 yr, which is considerably longer than that the 13,000 yr determined by
289 Ravishankara *et al.* (1993) despite our Lyman- α cross section (1.37×10^{-18} cm², **Table 1**) being
290 only ~22% smaller than the value the value measured by Ravishankara *et al.* (1.76×10^{-18} cm²).
291 One reason why our photolysis-related partial lifetime is longer is that WACCM includes
292 diffusive separation, which was not described in the earlier 2-D model study. The inclusion of
293 diffusive separation reduces sharply the abundance of SF₆ at high altitudes, where photolysis
294 is most effective. Another contributing factor could be that the VUV photolysis is important
295 only above 80 km, while in our model runs SF₆ is mostly destroyed by electron attachment,
296 which results in less being transported into this upper mesospheric region. When we analyse
297 our WACCM SF₆ tracer which is subject to photolysis loss only, the resulting steady-state
298 *overall* lifetime for the last model year (2007) is 17,200 yr which is only 32% larger than the
299 value of Ravishankara *et al.* (1993) and thus more consistent with the difference in the Lyman-
300 α cross sections. Finally, if we do not include the electron scaling factor to reduce the electron
301 density below 80 km due to negative ion formation, then the SF₆ lifetime decreases to 776 years
302 (not shown), which is similar to the value obtained by Morris *et al.* (1995).

303 **3.3 Impact of SF₆ loss on mean age of stratospheric air**

304 As SF₆ is a chemically stable molecule in the stratosphere and troposphere, and has an almost
305 linearly increasing tropospheric abundance, its atmospheric mixing ratio is often used to
306 determine the mean age of stratospheric air. This is an important metric in atmospheric science
307 as the distribution of ozone and other greenhouse gases depends significantly on the transport
308 of air into, within, and out of the stratosphere. WACCM contains an idealized, linearly-
309 increasing age-of-air tracer (AOA1) that provides model age values for model experiments
310 (Garcia *et al.*, 2011).

311 Age-of-air has generally been derived from observations by treating SF₆ as a passive (non-
312 reactive) tracer. The assumption is that the global loss rate is too slow to significantly affect
313 the lifetime. This was confirmed by Garcia *et al.* (2011) when only photolysis was included.
314 However, when loss via electron attachment is also considered, the lifetime may become short
315 enough that this assumption is no longer valid, in which case the stratospheric mixing ratio
316 would appear to correspond to an earlier tropospheric mixing ratio than in reality. We have



317 compared the passive WACCM SF₆ tracer with that subject to all loss processes, which yields
 318 the new lifetime of 1278 yr. The difference between these two tracers indicates the error in the
 319 derived age-of-air that would arise in the real atmosphere if SF₆ is assumed to be a passive
 320 tracer. The error caused by chemical removal can be expressed as:

$$321 \quad \Delta(\text{AoA}) = \text{AoA}(\text{reactive tracer}) - \text{AoA}(\text{passive tracer}) \quad (\text{E4})$$

322 where $\Delta(\text{AoA})$ is the difference in the age-of-air value caused by chemical loss, $\text{AoA}(\text{reactive}$
 323 $\text{tracer})$ is the calculated age-of-air considering the chemical removal, and $\text{AoA}(\text{passive tracer})$
 324 is the value obtained from a non-reactive tracer. The expression for the age-of-air at any point
 325 in the stratosphere can be obtained from a simplified version of (E1) that is derived from a
 326 Taylor series expansion, retaining only the linear term; then it is expressed as

$$327 \quad \text{AoA} = [(\chi_0(\text{SF}_6) - \chi(\text{SF}_6)) / r(\text{SF}_6)] \quad (\text{E5})$$

328 where $\chi(\text{SF}_6)$ and $\chi_0(\text{SF}_6)$ are the SF₆ volume mixing ratios at the actual and the reference
 329 (tropical tropopause) points, respectively, while $r(\text{SF}_6)$ is the rate of increase of tropospheric
 330 SF₆. In our simulations $r(\text{SF}_6)$ is 0.29 pptv/year (**Figure 4**), which is an approximation as the
 331 growth rate is not constant in reality. Stiller *et al.* (2012) report a value of 0.24 pptv/year based
 332 on observations. These two simplifications will lead to deviations between WACCM and
 333 MIPAS age data. If (E5) is substituted into (E4) then the error in age-of-air will be:

$$334 \quad \Delta(\text{AoA}) = (\chi(\text{SF}_{6, \text{passive}}) - \chi(\text{SF}_{6, \text{reactive}})) / r(\text{SF}_6) \quad (\text{E6})$$

335 This error, along with the mean age itself, was calculated from WACCM output for 2007.
 336 **Figure 7** shows the annual mean ages determined from the WACCM simulation from 2002-
 337 2007 using the total reactive and the inert SF₆ tracers and the idealized AOA1 age tracer. There
 338 is a clear difference between the age values derived from the passive SF₆ and the idealized AoA
 339 tracer. If equation (E5) is used to determine the age values there is no guarantee that the age
 340 values derived from the two tracers will be identical; the rate was determined from the increase
 341 of the SF₆ burden (0.29 pptv/year) and this was provided by the linear fit (**Figure 4**), which
 342 can misrepresent the growth rate at any time. **Figure 7** also shows the difference between the
 343 age values obtained from the reactive and inert SF₆ tracers. It can be seen that consideration of
 344 the reactive SF₆ tracer does indeed affect the determined mean age values, mostly where
 345 electron attachment dominates. The age estimates at high latitudes are most sensitive to
 346 chemical loss because the air that reaches these locations has descended from the high altitudes



347 where SF₆ loss predominantly occurs. According to the MIPAS satellite observations (Stiller
348 *et al.*, 2012; Haenel *et al.*, 2015.), the derived age value over the tropical lower stratosphere at
349 25 km is slightly more than 3 years, while the WACCM simulations with the reactive SF₆ tracer
350 predicts 3 years. Comparing **Figures 7a** and **7b**, the effect of chemical removal in this region
351 is minor (0.01 year or 0.5% change) and therefore it does not have much impact on the inferred
352 atmospheric transport. At the poles the effect is much more significant; the difference at 25 km
353 between the reactive and inert SF₆ tracers is up to 0.55 years (9%). This means that in the
354 troposphere-stratosphere low latitude regions the effect of chemical removal is not very
355 significant and the error on the estimated mean age caused by the assumption of SF₆ being a
356 passive tracer is not important. However, the effect of chemical removal becomes more
357 significant at high latitudes.

358 We can also compare modelled and observed mean age values in the lower stratosphere (20
359 km). **Figure 8** shows the mean age profiles from WACCM tracers, ER-2 observations (Hall *et*
360 *al.*, 2009) and our analysis of MIPAS SF₆ satellite data at 20 km. From this it can be seen that
361 in the tropical region the mean age values are similar between the idealized age tracer and the
362 inert and reactive SF₆ tracers. This is consistent with no loss of SF₆ having occurred in air
363 parcels in the deep tropics. At high latitudes there is up to 0.5 year difference in the modelled
364 mean ages, with the reactive SF₆ tracer producing the oldest apparent age. The differences in
365 mean age between the tracers is larger in the SH polar region than in the NH because the polar
366 region is less well mixed. The tendency is very similar when we compare the WACCM mean
367 ages to the MIPAS observations. Note that the satellite observations show more seasonal
368 variability in the middle and high latitudes than in the tropics.

369 **3.4 Radiative Efficiency and Forcing**

370 To determine the radiative efficiency and global warming potential of SF₆, integrated cross-
371 sections were taken from the GEISA: 2011 Spectroscopic Database (Varanasi, 2011), the
372 HITRAN 2012 Molecular Spectroscopic Database (Rothman *et al.*, 2012), and were also
373 measured in this study. The literature values are presented in **Table 4** for comparison with our
374 experimentally determined values and the full SF₆ spectrum obtained in this study is given in
375 **Figure 9**. In our study the spectrometer error is ±1.0% for all experiments, and the uncertainty
376 in the sample concentrations of SF₆ was calculated to be 0.7%. Spectral noise was averaged at
377 ±5×10⁻²¹ cm² molecule⁻¹ per 1 cm⁻¹ band. However, at wavenumbers <550 cm⁻¹, towards the
378 edge of the mid infrared where opacity of the KBr optics increases, this value was 1×10⁻²⁰ cm²



379 molecule⁻¹ per 1 cm⁻¹ band. The error from determining the scaling cross-section was 5%. This
380 results in an average overall error of ±5% in the cross-sections.

381 The intensities of the main SF₆ absorption bands (925-955 cm⁻¹) measured in this study are 7%
382 greater than those reported by (Hurley, 2003), 1% greater than GEISA (Varanasi, 2011) and 1%
383 lower than those given in HITRAN (Rothman *et al.*, 2012) (**Table 4**). Comparison of our results
384 against Varanasi (2011) between 650 and 2000 cm⁻¹ gives an agreement within 9%. Note that
385 these differences are within the combined error of both experiments.

386 The instantaneous and stratospheric adjusted SF₆ radiative efficiencies in clear and cloudy sky
387 conditions are given in **Table 5**. These are also presented as present-day radiative forcings
388 employing a current surface concentration of 9.3 pptv (NOAA, 2016) (see **Figure 4**). The
389 radiative efficiency was calculated in the RFM for each month between 90°S and 90°N at
390 latitudinal resolutions (on which the data was averaged to obtain the zonal mean vertical
391 profile) of 1.5° and 9.0°. The tropopause used the standard WMO lapse rate definition (see
392 Totterdill *et al.*, 2016). **Figure 10** shows the seasonal-latitudinal variation of the instantaneous
393 clear sky radiative forcing for SF₆ on the high (1.5°) and low (9°) resolution grids. Employing
394 profiles averaged over the lower resolution grid gives an average forcing within 1% of the
395 higher resolution grid. Using only a single annually averaged global mean profile led to a 10%
396 error in radiative forcing when compared to our monthly resolved high resolution profile,
397 supporting the findings of Freckleton *et al.* (1998) and Totterdill *et al.* (2016).

398 A selection of experiments were carried out over a range of months and latitudes to investigate
399 the sensitivity of the forcing calculations to the bands used. The average contributions from the
400 main bands were compared against the calculation with the full measured spectrum. The results
401 showed that the 580 – 640 and 925 – 955 cm⁻¹ bands contribute almost 99% to the instantaneous
402 radiative forcing. Our forcing calculations suggest that the SF₆ minor bands contribute only a
403 small amount to the final value. This means that deviations between our experimentally
404 determined spectra and those in the literature only result in a significant change to previously
405 published radiative forcings and efficiencies when that deviation occurs over a major band.

406 The SF₆ adjusted cloudy sky radiative efficiency published by the IPCC AR5 report and used
407 to determine its GWP values is 0.57 Wm⁻² ppbv⁻¹ (Myhre *et al.*, 2013). This compares to the
408 adjusted cloudy sky radiative efficiency determined in this study of 0.59 Wm⁻² ppbv⁻¹. A review
409 on radiative efficiencies and global warming potentials by Hodnebrog *et al.* (2013) provides a



410 comprehensive list of all published values for these parameters for many species including SF₆.
411 They established the range of published radiative efficiencies for SF₆ to be 0.59 – 0.68 Wm⁻²
412 ppbv⁻¹, with a mean value of 0.56 Wm⁻² ppbv⁻¹. They also made their own revised estimate
413 using an average of the HITRAN (Rothman *et al.*, 2012) and GEISA (Hurley, 2003; Varanasi,
414 2011) spectral databases and found a best estimate of (0.565 ± 0.025) Wm⁻² ppbv⁻¹. Their mean
415 value for radiative efficiency is very close to that determined in this study using similar
416 conditions (0.59 Wm⁻² ppbv⁻¹).

417 **3.5 Global Warming Potential**

418 **Table 6** gives our estimates of the 20, 100 and 500-year GWPs based on cloudy sky adjusted
419 radiative efficiencies of SF₆ compared with IPCC AR5 values (IPCC, 2013). Our 20, 100 and
420 500-year global warming potentials for SF₆ are 18,000, 23,800 and 31,300 respectively. The
421 20-year and 100-year values are 3% greater and 1% greater, respectively, than their IPCC
422 counterparts and the 500-year GWP is 4% smaller than its AR4 counterpart (Forster *et al.*,
423 2007). Forcing efficiencies determined in this study are somewhat higher than previously
424 published values, which imply a higher value for GWP. However, our shorter atmospheric
425 lifetimes would lead to a smaller GWP estimate. The trade-off between these competing effects
426 is apparent in **Table 6**, where SF₆ exhibits a 20-year GWP that is slightly larger than the IPCC
427 value, while the 500-year GWP is slightly smaller. The radiative efficiency effect is most
428 obvious for the case of the 20-year GWP where, because the atmospheric lifetime of SF₆ is
429 1278 years, the species does not have time for any significant loss to occur.

430 **4 Conclusions**

431 The 3D Whole Atmosphere Community Climate Model was used to simulate the SF₆
432 atmospheric distribution over the period of 1995-2007. From the concentrations and the
433 knowledge of the electron attachment, photolysis and metal reaction rates we determined the
434 atmospheric lifetime which shows a significant dependence on the solar cycle due to varying
435 electron density. The mean SF₆ atmospheric lifetime and 1σ variation over a solar cycle were
436 determined to be 1278 years (ranging from 1120 to 1475 years), which is different to previously
437 reported literature values and much shorter than the widely quoted value of 3200 years. The
438 reason is our more detailed treatment of electron attachment using a new formalism to describe
439 both associative and dissociative attachment, and the use of a detailed model of D region ion
440 chemistry to evaluate the partitioning of electrons and negative ions below 80 km.



441 Based on this new estimate of the SF₆ lifetime, we find that the derived mean age of
442 stratospheric air from observations can be slightly affected by the atmospheric removal of SF₆.
443 In the polar region the age-of-air values differ by up to 9% when the values from inert and
444 reactive model tracers are compared, suggesting that SF₆ loss does not have a large influence
445 on the age values but that it should be included in detailed analyses.

446 We also re-investigated the radiative efficiency and global warming potential of SF₆. Our
447 radiative efficiency value reported here, $0.59 \pm 0.045 \text{ Wm}^{-2} \text{ ppbv}^{-1}$, is slightly higher than the
448 IPCC AR5 estimate of $0.57 \text{ Wm}^{-2} \text{ ppbv}^{-1}$. The global warming potentials of SF₆ for 20, 100
449 and 500 years have been determined to be 18,000, 23,800 and 31,300, respectively. We find
450 that our revised lifetime and efficiency values somewhat cancel each other out so overall do
451 not play a significant role in modifying the GWP estimates.

452 **Acknowledgements**

453 This work was part of the MAPLE project funded by research grant NE/J008621/1 from the
454 UK Natural Environment Research Council, which also provided a studentship for AT. The
455 authors are also thankful to Prof Jürgen Troe for the helpful discussions related to the electron
456 attachment to SF₆.



457 **References**

- 458 Chabrilat, S. and Kockarts, G.: Simple parameterization of the absorption of the solar Lyman-
459 alpha line, *Geophys. Res. Lett.*, 24, 2659-2662, 1997.
- 460 Dudhia, A.: Reference Forward Model V4.30: <http://www.atm.ox.ac.uk/RFM>, 2013.
- 461 Edwards, D. P.: GENLN2: The new Oxford line-by-line atmospheric transmission/radiance
462 model, Clarendon Laboratory, Oxford, 1987.
- 463 Freckleton, R. S., Highwood, E. J., Shine, K. P., Wild, O., Law, K. S., and Sanderson, M. G.:
464 Greenhouse gas radiative forcing: Effects of averaging and inhomogeneities in trace gas
465 distribution, *Q. J. Roy. Meteor. Soc.*, 124, 2099-2127, 10.1002/qj.49712455014, 1998.
- 466 Forster, P., V. Ramaswamy, P. Artaxo, T. Berntsen, R. Betts, D.W. Fahey, J. Haywood, J.
467 Lean, D.C. Lowe, G. Myhre, J. Nganga, R. Prinn, G. Raga, M. Schulz and R. Van
468 Dorland: Changes in Atmospheric Constituents and in Radiative Forcing. *In: Climate
469 Change 2007: The Physical Science Basis. Contribution of Working Group I to the Fourth
470 Assessment Report of the Intergovernmental Panel on Climate Change*, Cambridge
471 University Press, Cambridge, United Kingdom and New York, NY, USA, 2007.
- 472 Garcia, R. R., Randel, W. J., and Kinnison, D. E.: On the determination of age of air trends
473 from atmospheric trace species, *J. Atmos. Sci.*, 68, 139-154, 2011.
- 474 Garcia, R. R., López-Puertas, M., Funke, B., Marsh, D. R., Kinnison, D. E., Smith, A. K. and
475 González-Galindo, F.: On the distribution of CO₂ and CO in the mesosphere and lower
476 thermosphere, *J. Geophys. Res.*, 119, 5700-5718, 2014.
- 477 Geller, L. S., Elkins, J. W., Lobert, J. M., Clarke, A. D., Hurst, D. F., Butler, J. H., and Myers,
478 R. C.: Tropospheric SF₆: Observed latitudinal distribution and trends, derived emissions and
479 interhemispheric exchange time, *Geophys. Res. Lett.*, 24, 675-678, 1997.
- 480 Haedel, F.J., Stiller, G.P., von Clarmann, T., Funke, B., Eckert, E., Glatthor, N., Grabowski,
481 U., Kellmann, S., Kiefer, M., Linden, A. and Reddman, T.: Reassessment of MIPAS age
482 of air trends and variability, *Atmos. Chem. Phys.*, 15, 13161-13176, 2015.
- 483 Hall, T.M., and Plumb, R.A.: Age as a diagnostic of stratospheric transport. *J. Geophys. Res.*,
484 99, 1059-1070, 1994.
- 485 Hall, T. M., Waugh, D. W., Boering, K. A., and Plumb, R. A.: Evaluation of transport in
486 stratosphere models, *J. Geophys. Res.*, 104, 18815-18839, 1999.
- 487 Harnisch, J., and Eisenhauer, A.: Natural CF₄ and SF₆ on Earth, *Geophys. Res. Lett.*, 25, 2401-
488 2404, 1998.



- 489 Hodnebrog, Ø., Etminan, M., Fuglestedt, J. S., Marston, G., Myhre, G., Nielsen, C. J., Shine,
490 K. P., and Wallington, T. J.: Global warming potentials and radiative efficiencies of
491 halocarbons and related compounds: A comprehensive review, *Rev. Geophys.*, 51, 300-378,
492 10.1002/rog.20013, 2013.
- 493 Hurley, M. D.: GEISA : 2011 Spectroscopic Database; SF₆ Infrared Absorption Cross-sections,
494 2003.
- 495 IPCC: Climate Change 2013: The Physical Science Basis. Contribution of Working Group I to
496 the Fifth Assessment Report of the Intergovernmental Panel on Climate Change, Cambridge
497 University Press, Cambridge, United Kingdom and New York, NY, USA, 1535 pp., 2013.
- 498 Kovács, T., Feng, W., Plane, J. M. C., Chipperfield, M. P., Nagy, T., Verronen, P. T.,
499 Andersson, M., Newnham, D., Clilverd, M., and Marsh, D. R.: D-region ion-neutral coupled
500 chemical model, *Geosci. Model Dev.*, (submitted), 2016.
- 501 Lamarque, J.-F., Emmons, L. K., Hess, P. G., Kinnison, D. E., Tilmes, S., Vitt, F., Heald, C.
502 L., Holland, E. A., Lauritzen, P. H., Neu, J., Orlando, J. J., Rasch, P., and Tyndall, G.: CAM-
503 chem: description and evaluation of interactive atmospheric chemistry in CESM., *Geosci.*
504 *Model Dev.*, 5, 369-411, 2012.
- 505 Maiss, M., and Brenninkmeijer, C. A. M.: Atmospheric SF₆, trends, sources and prospects.,
506 *Environ. Sci. Technol.*, 32, 3077-3086, 1998.
- 507 Marsh, D. R., Mills, M. J., Kinnison, D. E., and Lamarque, J.-F.: Climate change from 1850 to
508 2005 simulated in CESM1 (WACCM), *J. Climate*, 26, 7372-7391, 2013.
- 509 Mayer, and Kylling: Technical note: The libRadtran software package for radiative transfer
510 calculations - description and examples of use, *Atmos. Chem. Phys.*, 5, 1855-1877, 2005.
- 511 Meredith, N. P., Horne, R. B., Isles, J. D., and Rodriguez, J. V.: Extreme relativistic electron
512 fluxes at geosynchronous orbit: Analysis of GOES E > 2 MeV electrons, *Space Weather*,
513 13, 170-184, 2015.
- 514 Morris, R. A., Miller, T. M., Viggiano, A. A., Paulson, J. F., Solomon, S., and Reid, G.: Effects
515 of electron and ion reactions on atmospheric lifetimes of fully fluorinated compounds, *J.*
516 *Geophys. Res.*, 100, 1287-1294, 1995.
- 517 Myhre, G., Shindell, D., Bréon, F.-M., Collins, W., Fuglestedt, J., Huang, J., Koch, D.,
518 Lamarque, J.-F., Lee, D., Mendoza, B., Nakajima, T., Robock, A., Stephens, G., Takemura,
519 T., and Zhang, H.: Anthropogenic and natural radiative forcing, Cambridge (UK), New
520 York (USA), 2013.



- 521 NOAA Earth System Research Laboratory, Halocarbons and other atmospheric trace gases,
522 SF₆ – Combined Dataset, <http://www.esrl.noaa.gov/gmd/hats/combined/SF6.html>,
523 [Accessed 1/1/2016], 2016.
- 524 Plane, J. M. C., Feng, W., and Dawkins, E. C. M.: The mesosphere and metals, *Chem. Rev.*,
525 115, 4497-4541, 2015.
- 526 Ravishankara, A. R., Solomon, S., Turnipseed, A. A., and Warren, R. F.: Atmospheric lifetimes
527 of long-lived halogenated species, *Science*, 259, 194-199, 1993.
- 528 Reddman, T., Ruhnke, R., and W. Kouker, W.: Three-dimensional model simulations of SF₆
529 with mesospheric chemistry, *J. Geophys. Res.*, 106, 14,525–14,537,
530 doi:10.1029/2000JD900700, 2001.
- 531 Rothman, L. S., Gordon, I. E., Babikov, Y., Barbe, A., Benner, D. C., Bernath, P. F., Birk, M.,
532 Bizzocchi, L., Boudon, V., Brown, L. R., Campargue, A., Chance, K., Cohen, E. A.,
533 Coudert, L. H., Devi, V. M., Drouin, B. J., Faytl, A., Flaud, J. M., Gamache, R. R., Harrison,
534 J. J., Hartmann, J. M., Hill, C., Hodges, J. T., Jacquemart, D., Jolly, A., Lamouroux, J., Roy,
535 R. J. L., Li, G., Long, D. A., Lyulin, O. M., Mackie, C. J., Massie, S. T., Mikhailenko, S.,
536 Müller, H. S. P., Naumenko, O. V., Nikitin, A. V., Orphal, J., Perevalov, V., Perrin, A.,
537 Polovtseva, E. R., Richard, C., Smith, M. A. H., Starikova, E., Sung, K., Tashkun, S.,
538 Tennyson, J., Toon, G. C., Tyuterev, W. G., and Wagner, G.: The HITRAN 2012 Molecular
539 Spectroscopic Database, *J. Quant. Spectrosc. Radiat. Transfer*, 4 - 50, 2012.
- 540 Stamnes, K., Tsay, S. C., Wiscombe, W., and Laszlo, I.: DISORT, a General-Purpose Fortran
541 Program for Discrete-Ordinate-Method Radiative Transfer in Scattering and Emitting
542 Layered Media: Documentation of Methodology, 2000.
- 543 Stiller, G. P., von Clarmann, T., Höpfner, M., Glatthor, N., Grabowski, U., Kellmann, S.,
544 Kleinert, A., Linden, A., Milz, M., Reddman, T., Steck, T., Fischer, H., Funke, B., Lopez-
545 Puertas, M., and Engel, A.: Global distribution of mean age of stratospheric air from MIPAS
546 SF₆ measurements, *Atmos Chem Phys*, 8, 677–695, 2008.
- 547 Stiller, G. P., von Clarmann, T., Haanel, F., Funke, B., Glatthor, N., Grabowski, U., Kellmann,
548 S., Kiefer, M. Linden, A., Lossow, S. and López-Puertas, M.: Observed temporal evolution
549 of global mean age of stratospheric air for the 2002 to 2010 period, *Atmos. Chem. Phys.*,
550 12, 3311-3331, 2012.
- 551 Tapping, K. E.: The 10.7 cm solar radio flux (F10.7), *Space Weather*, 11, 394-406, 2013.



- 552 Totterdill, A., Kovács, T., Gomez-Martin, J. C., Feng, W., and Plane, J. M. C.: Mesospheric
553 removal of very long-lived greenhouse gases SF₆ and CFC-115 by metal reactions, Lyman-
554 α photolysis, and electron attachment, *J. Phys. Chem. A*, 115, 2016-2025, 2015.
- 555 Totterdill, A., Kovács, T., Feng, W., Dhormse, S., Smith, C., Martin, J. C. G., Chipperfield,
556 M., Forster, P., and Plane, J.: Atmospheric Lifetimes, Infrared Absorption Spectra,
557 Radiative Forcings and Global Warming Potentials of NF₃ and CFC-115, *Atmos. Chem.*
558 *Phys.*, (submitted), doi:10.5194/acp-2016-231, 2016.
- 559 Troe, J., Miller, T. M., and Viggiano, A. A.: Low-energy Electron Attachment to SF₆. I. Kinetic
560 modeling of nondissociative attachment, *J. Chem. Phys.*, 127, 244303, 2007a.
- 561 Troe, J., Miller, T. M., and Viggiano, A. A.: Low-energy electron attachment to SF₆. II.
562 Temperature and pressure dependences of dissociative attachment, *J. Chem. Phys.*, 127,
563 244304, 2007b.
- 564 Varanasi, P. and M.D. Hurley. SF₆ Infrared Absorption Cross-Sections. 2011 [Accessed
565 03/03/2015] Available from:
566 http://ether.ipsl.jussieu.fr/ether/pubipsl/GEISA/geisa_crossIR_frame_2011_uk.jsp.
- 567 Verronen, P. T., Seppälä, A., Clilverd, M. A., Rodger, C. J., Kyrölä, E., Enell, C.-F., Ulich, T.,
568 and Turunen, E.: Diurnal variation of ozone depletion during the October-November 2003
569 solar proton events, *J. Geophys. Res.*, 110, A09S32, 2005.
- 570 Viggiano, A. A., Miller, T. M., Friedman, J. F., and Troe, J.: Low-energy electron attachment
571 to SF₆. III. From thermal detachment to the electron affinity of SF₆, *J. Chem. Phys.*, 127,
572 244305, 2007.
- 573 Waugh, D., and Hall, T: Age of stratospheric air: Theory, observations and models, *Rev*
574 *Geophys.*, 40, doi:10.1029/2000RG000101, 2002.
- 575



576 **Tables**

577 **Table 1.** SF₆ loss reactions included in WACCM.

Loss process	Rate constant	Reference and comments
Na + SF ₆	$k = 1.80 \times 10^{-11} \exp(-590.5/T)$	From Totterdill <i>et al.</i> , (2015) Refitted for mesospheric temperatures 215-300K.
K + SF ₆	$k = 13.4 \times 10^{-11} \exp(-860.6/T)$	From Totterdill <i>et al.</i> , (2015) Refitted for mesospheric temperatures 215-300K.
Electron attachment	Associative attachment: $k_{EA,ass} = k_{at} \times (k_{(SF_6^- + H)}[H] + k_{(SF_6^- + HCl)}[HCl]) / (j_{PD} + k_{(SF_6^- + H)}[H] + k_{(SF_6^- + HCl)}[HCl] + k_{(SF_6^- + O_3)}[O_3] + k_{(SF_6^- + O)}[O])$ Dissociative attachment: $k_{EA,diss} = k_{at} \times \beta$, where β is the fraction of SF ₆ ⁻ that dissociates into SF ₅ ⁻ .	Totterdill <i>et al.</i> , (2015).
Photolysis	Lyman- α : $\sigma(121.6 \text{ nm}) = 1.37 \times 10^{-18} \text{ cm}^2$ Parameterised expression over the range of 115-180 nm, based on previous measurements.	Totterdill <i>et al.</i> , (2015).

578

579 **Table 2.** Positive and negative ions included in WACCM-SIC.

Positive ions	O_2^+ , O_4^+ , NO^+ , $NO^+(H_2O)$, $O_2^+(H_2O)$, $H^+(H_2O)$, $H^+(H_2O)_2$, $H^+(H_2O)_3$, $H^+(H_2O)_4$, $H^+(H_2O)_5$, $H^+(H_2O)_6$, $H_3O^+(H_2O)_2(CO_2)$, $H_3O^+(OH)$, $O_2^+(CO_2)$, $H_3O^+(OH)(CO_2)$, $H_3O^+(OH)(H_2O)$, $O_2^+(H_2O)(CO_2)$, $O_2^+(H_2O)_2$, $O_2^+(N_2)$, $NO^+(H_2O)_2$, $H^+(H_2O)(CO_2)$, O^+ , N^+ , N_2^+ , $NO^+(H_2O)_3$, O_4^+ , $H^+(H_2O)_2(CO_2)$, $H^+(H_2O)_2(N_2)$
Negative ions	O_3^- , O^- , O_2^- , OH^- , $O_2^-(H_2O)$, $O_2^-(H_2O)_2$, O_4^- , CO_3^- , $CO_3^-(H_2O)$, CO_4^- , HCO_3^- , NO_2^- , NO_3^- , $NO_3^-(H_2O)$, $NO_3^-(H_2O)_2$, $NO_3^-(HNO_3)$, NO_3^- $(HNO_3)_2$, Cl^- , ClO^- , $NO_2^-(H_2O)$, $Cl^-(H_2O)$, $Cl^-(CO_2)$, $Cl^-(HCl)$

580

 581 **Table 3.** Partial (reactions with electrons, photolysis, and metals (K, Na)) and total atmospheric
 582 lifetimes (years) of SF_6 from different studies. Numbers in parentheses show relative
 583 percentage contribution of loss due to the different processes.

Study	Lifetime / years			Model dimensions
	Photolysis	Electron attachment	Total	
Ravishankara <i>et al.</i> (1993)	13,000 (24%)	4210 (76%)	3200	2D
Morris <i>et al.</i> (1995)	N/A	N/A	800	2D
This work	48,000 (2.6%)	1339 (97.4%)	1278	3D

584



585 **Table 4.** Integrated absorption cross-sections for SF₆ measured in this work and ratios with
 586 values obtained by Hurley (2003), Varanasi (2001) and HITRAN (Rothman *et al.*, 2012).

Band limits (cm ⁻¹)	Integrated cross-section (10 ⁻¹⁶ cm ² molec ⁻¹ cm ⁻¹)	Ratio of integrated cross-sections in this work to previous studies		
		Hurley (2003)	Varanasi (2001)	HITRAN
925 - 955	2.02	1.07	1.01	0.99
650 - 2000	2.40	-	1.09	-

587

588 **Table 5.** Calculated instantaneous and stratospheric adjusted radiative forcings and radiative
 589 efficiencies of SF₆ in clear and all-sky conditions^a.

	Instantaneous		Stratospheric adjusted	
	Clear	All-sky	Clear	All-sky
Radiative forcing (mWm ⁻²)	76.43	48.91	81.81	56.01
Radiative efficiency (Wm ⁻² ppbv ⁻¹)	0.77	0.50	0.85	0.59

590 a. Based on present day atmospheric SF₆ surface concentration of 9.3 pptv.

591 **Table 6.** Comparison of 20, 100 and 500-year global warming potentials for SF₆ from this work
 592 with values from IPCC (2013).

	Global Warming Potential		
	GWP ₂₀	GWP ₁₀₀	GWP ₅₀₀
This work ^a	18000	23700	31300
IPCC (2013) ^b	17500	23500	32600 ^c
Difference (%) (This work – IPCC)	+3%	+1%	-4%

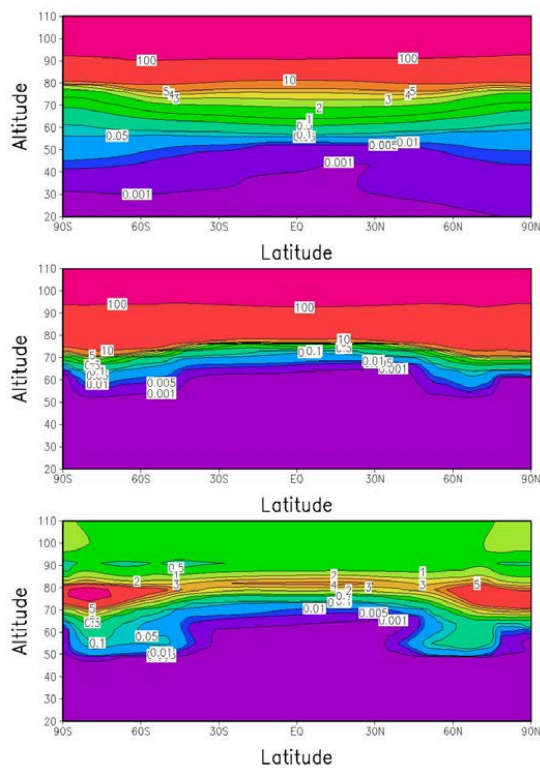
593 ^a Based on our atmospheric lifetime of 1278 yrs and RE of 0.59 Wm⁻² ppbv⁻¹.

594 ^b Based on an atmospheric lifetime of 3200 yrs and RE of 0.57 Wm⁻² ppbv⁻¹.

595 ^c Based on an atmospheric lifetime of 3200 yrs and RE of 0.52 Wm⁻² ppbv⁻¹ from IPCC AR4
 596 (Forster *et al.*, 2007).



597 **Figures**

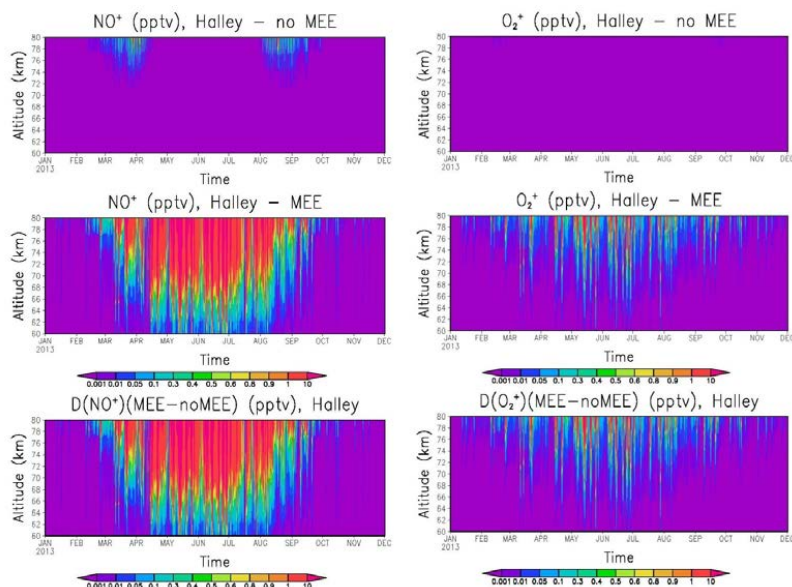


598

599 **Figure 1.** Top: annual average electron concentration for 2013 from the standard WACCM
600 model (in 10^2 electrons cm^{-3}). Middle: annual average electron concentration for 2013 from
601 WACCM-SIC model (in 10^2 electrons cm^{-3}). Bottom: annually averaged electron scaling factor
602 for 2013.



603

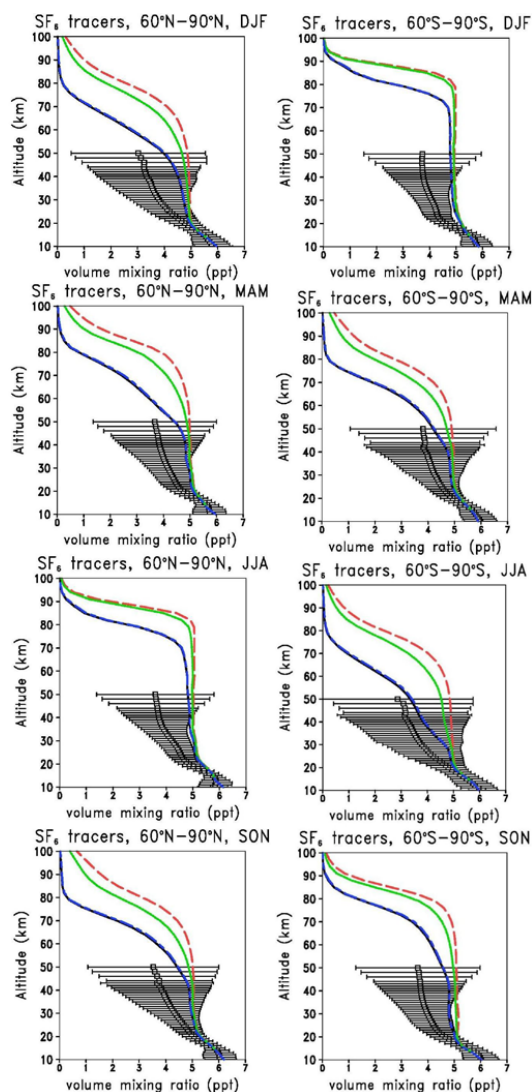


604

605 **Figure 2.** Time series of volume mixing ratio profiles (pptv) of NO^+ (left panels) and O_2^+ (right
606 panels) above Halley (76°S) from two WACCM-SIC simulations. Top panels show the values
607 obtained from the model run without medium energy electrons; the middle panels show the run
608 with medium energy electrons; and the bottom panels show the absolute differences between
609 the two model runs.



610

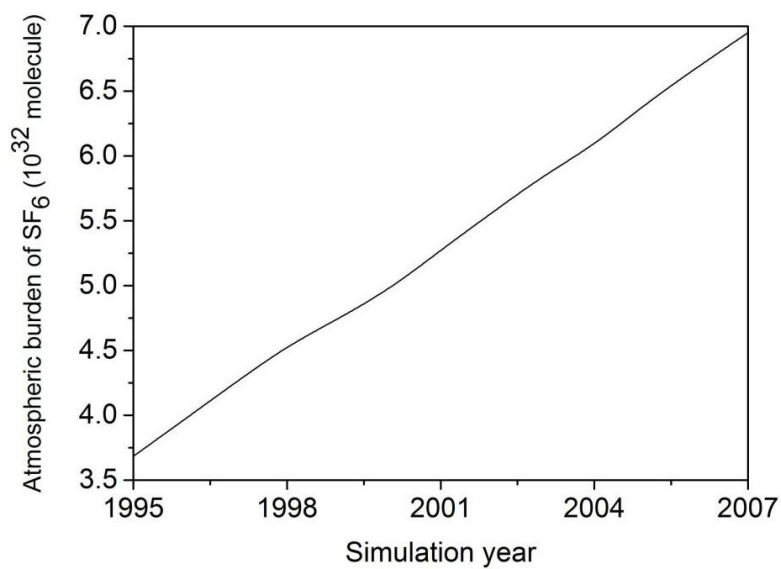


611

612 **Figure 3.** Annual volume mixing ratios (pptv) of the different SF₆ tracers for the polar regions
613 (60°N – 90°N and 60°S – 90°S latitudes) in 2007 as a function of altitude for MIPAS satellite
614 observed SF₆ (black symbols with standard deviations for $\pm 1\sigma$) (Stiller *et al.*, 2012), the total
615 WACCM-SF₆ (blue solid line), the photolysis WACCM-SF₆ tracer (green solid line) and the
616 inert WACCM SF₆ tracer (red dashed line).



617

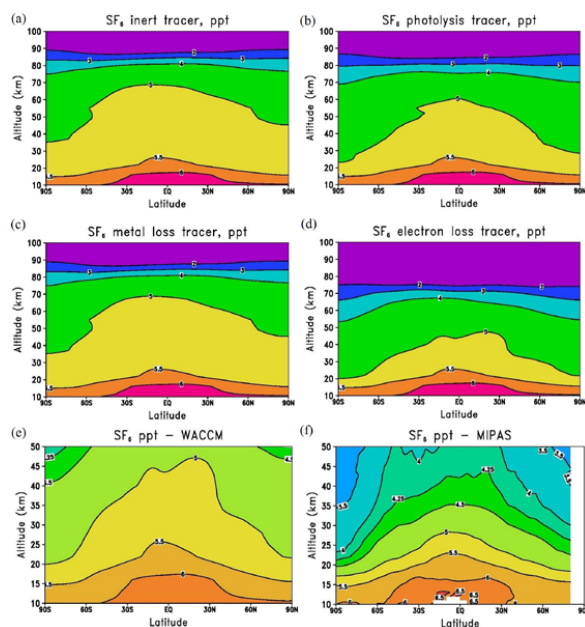


618

619 **Figure 4.** Variation of the total annual atmospheric burden of SF₆ during the simulation from

620 1995 to 2007. According to this the emission rate (slope) was determined to be 6.5×10^{-3}

621 Tg/year, corresponding to 0.29 pptv/year.

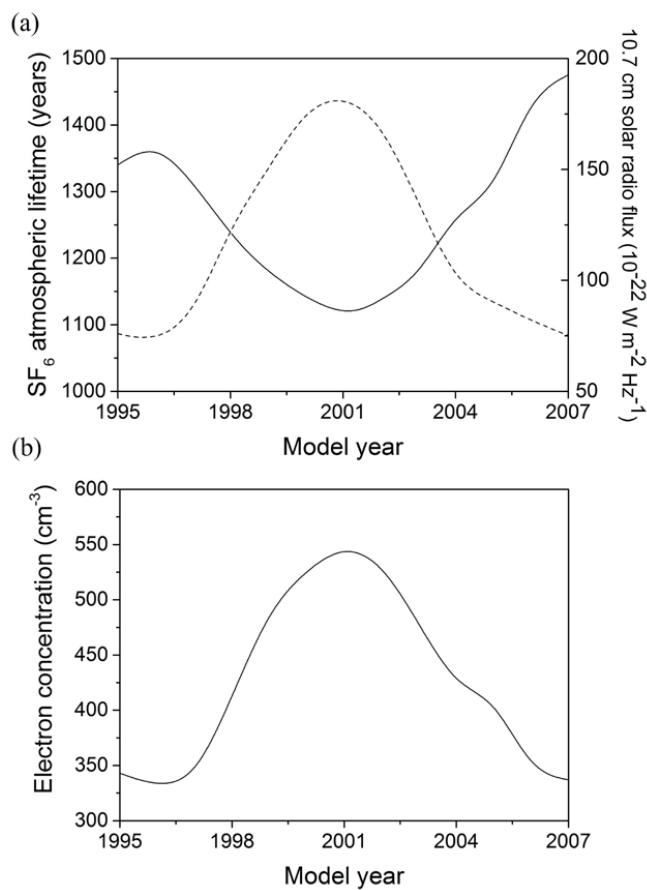


622

623 **Figure 5.** Annual zonal mean latitude-height volume mixing ratios (pptv) of the different
624 WACCM SF₆ tracers in 2007: (a) inert SF₆ tracer; (b) SF₆ tracer removed by photolysis only;
625 (c) SF₆ tracer removed by mesospheric metals only; (d) SF₆ tracer removed by electron
626 attachment only; and (e) total reactive SF₆. Panel (f) shows the SF₆ volume mixing ratio for
627 2007 from MIPAS observations. Note the different altitude ranges for panels (a)-(d) and (e)-
628 (f).

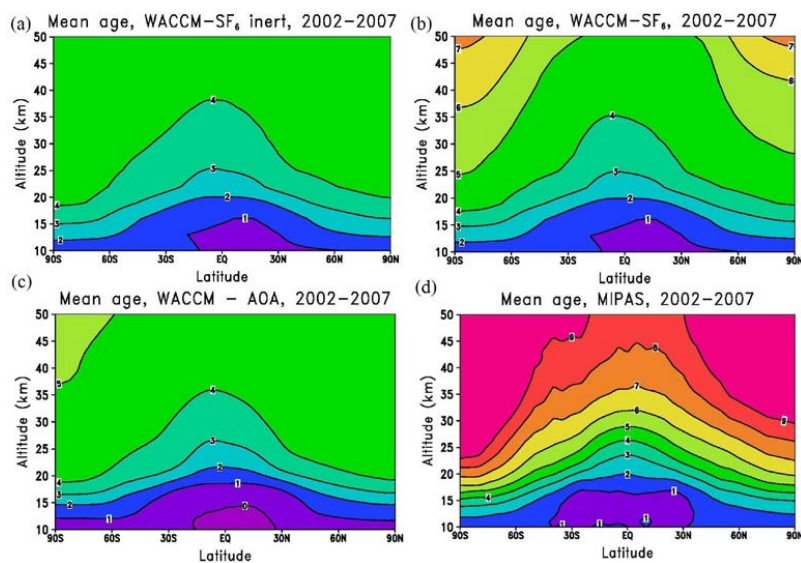


629



630

631 **Figure 6.** (a) Variation in atmospheric lifetime of SF₆ (solid line) and 10.7 cm solar radio flux
632 (dashed line) during the WACCM simulation. (b) Variation of the WACCM electron
633 concentration (cm⁻³) at 80 km, averaged over polar latitudes (60°N – 90°N and 60°S – 90°S).

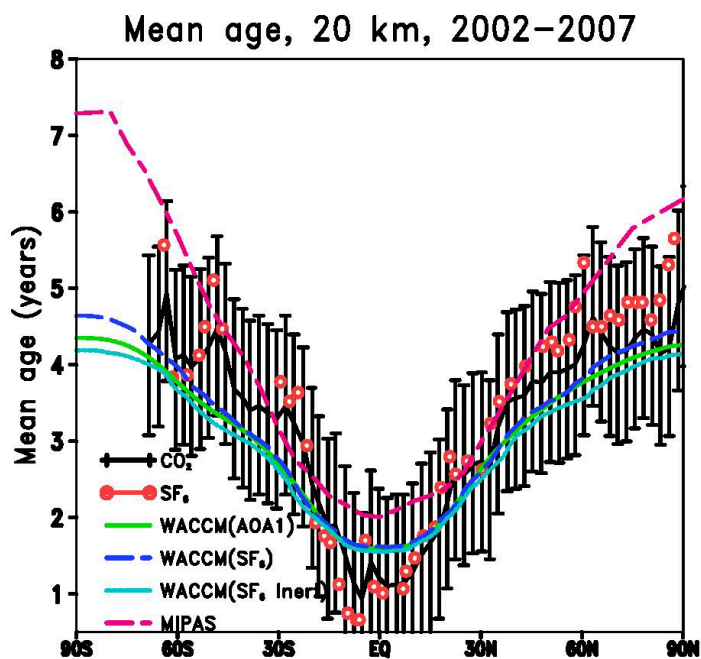


634

635 **Figure 7.** Annual mean age of stratospheric air (years) for the period of 2002–2007 determined
636 from a WACCM simulation using: (a) the inert SF₆ tracer; (b) the total reactive SF₆ tracer; (c)
637 the idealized AOA1 tracer. Panel (d) shows the age values derived for the same period from
638 our analysis of MIPAS SF₆ observations.



639



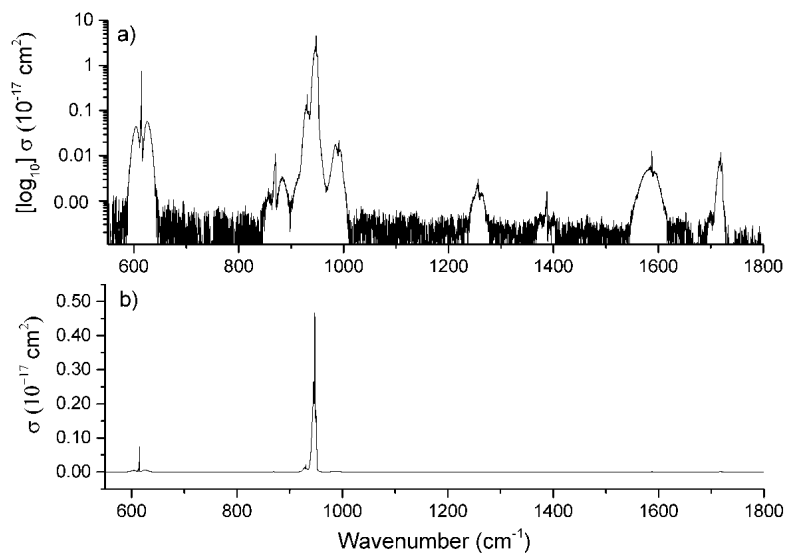
640

641 **Figure 8.** Mean age values at 20 km altitude derived from MIPAS satellite (dashed magenta
642 line) and ER-2 aircraft observations (SF₆ red open circles, CO₂ black crosses) (Hall *et al.*,
643 1999). The error bars apply to the age derived from the ER-2 observations. Also shown is the
644 mean age derived from WACCM tracers: reactive SF₆ (dashed blue line), passive SF₆ (light
645 blue line) and AOA tracer (solid green line).



646

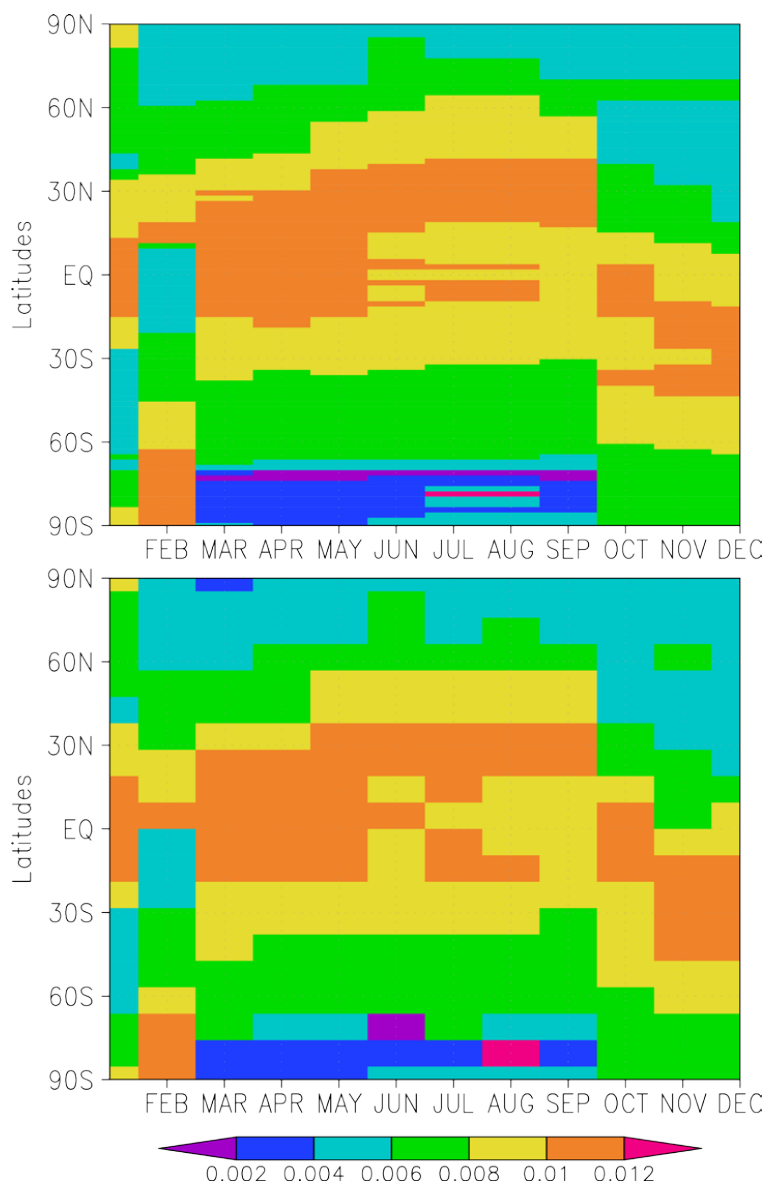
647



648

649

650 **Figure 9.** Infrared absorption spectrum of SF₆ at ~295 K on (a) a logarithmic y axis and (b) a
651 linear y axis. The logarithmic scale in panel (a) highlights the relative positions of the minor
652 bands.



653

654 **Figure 10.** Latitude-time plots for instantaneous radiative forcing (Wm^{-2}) by SF_6 as a function
655 of latitude and month at (a) high latitude resolution (1.5° spacing) and (b) low latitude
656 resolution (9° spacing).